

PolyKAN: Efficient Fused GPU Operators for Polynomial Kolmogorov–Arnold Network Variants

Mingkun Yu
Sun Yat-sen University
Guangzhou, China

Heming Zhong
Sun Yat-sen University
Guangzhou, China

Dan Huang
Sun Yat-sen University
Guangzhou, China

Yutong Lu
Sun Yat-sen University
Guangzhou, China

Jiazhi Jiang
Sun Yat-sen University
Guangzhou, China

Abstract

Kolmogorov–Arnold Networks (KANs) promise higher expressive capability and stronger interpretability than Multi-Layer Perceptron, particularly in the domain of AI for Science. However, practical adoption has been hindered by low GPU utilization of existing parallel implementations. To address this challenge, we present a GPU-accelerated operator library, named PolyKAN which is the first general open-source implementation of KAN and its variants. PolyKAN fuses the forward and backward passes of polynomial KAN layers into a concise set of optimized CUDA kernels. Four orthogonal techniques underpin the design: (i) *lookup-table* with linear interpolation that replaces runtime expensive math-library functions; (ii) *2D tiling* to expose thread-level parallelism with preserving memory locality; (iii) a *two-stage reduction* scheme converting scattered atomic updates into a single controllable merge step; and (iv) *coefficient-layout reordering* yielding unit-stride reads under the tiled schedule. Using a KAN variant, Chebyshev KAN, as a case-study, PolyKAN delivers 1.2–10× faster inference and 1.4–12× faster training than a Triton + cuBLAS baseline, with identical accuracy on speech, audio-enhancement, and tabular-regression workloads on both highend GPU and consumer-grade GPU.

Keywords: Kolmogorov–Arnold Networks, GPU operator optimization, CUDA fused kernels, deep-learning acceleration

1 Introduction

Deep learning (DL) has achieved remarkable progress across domains such as computer vision, natural language processing, and scientific computing [14]. Multilayer perceptrons (MLPs) [20] are foundational building blocks of deep learning, yet their inherently opaque nature raises concerns about transparency and interpretability [5, 19]. To pursue more accuracy and higher interpretability, researchers are compelled to explore novel model architectures and activation mechanisms of deep learning. As illustrated in Figure 1, traditional MLP employs fixed non-linear activation functions such as ReLU [16], Sigmoid [20] and Tanh [9]. In contrast, Kolmogorov–Arnold Network (KAN) [15] replaces the fixed activation functions with a linear combination of a set of polynomial basis functions, based on Kolmogorov–Arnold representation theorem [13]. The specific pattern of linear combination is determined by a set of learnable coefficients. Therefore, the process of mapping the input to the output through the nonlinear activation function is transparent.

KANs offer improved memory capacity, interpretability, and accuracy compared to traditional MLPs [31]. Therefore, KANs have been successfully extended to reconstruct various neural network modules, including convolutional [3], graph architectures [32], even Transformer [29] and large language models [7]. Especially in the domain of AI for Computational Science and Engineering such as partial differential equation [6], KAN has shown much better performance than MLP due to its characteristics [11, 25, 30]. To adapt to different tasks, KANs can further enhance the capability through adjusting basis functions and parameterization configurations. This prompts a wide spectrum of KAN variants based on Fourier [28], Chebyshev [21], Legendre [2], and other basis functions.

Although KAN variants possess these unique advantages, they typically suffer from 10× slower runtimes than MLPs with comparable model and parameter sizes [15]. This inefficiency stems from: (i) the use of parameterized univariate functions as activation function substantially increases computational overhead, (ii) KAN basis-expansion primitives use naive loop-based implementation, limited optimization for parallelism strategies, such as kernel fusion, and (iii) irregular memory access limits GPU concurrency. Convolutional

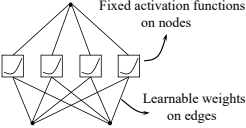
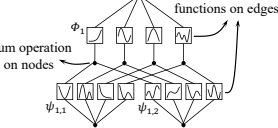
Model	Multi-Layer Perceptron(MLP)	Kolmogorov–Arnold Network(KAN)
Theorem	Universal Approximation Theorem	Kolmogorov–Arnold Representation Theorem
Formula	$MLP(x) \approx \sum_{i=1}^{N(e)} a_i \sigma(w_i \cdot x + b_i)$	$KAN(x) = \sum_{q=1}^{2n+1} \phi_q \left(\sum_{p=1}^n \psi_{q,p}(x_p) \right)$ Including Basis Function
Structure		

Figure 1. Architectural and theoretical comparison between traditional multi-layer perceptron (MLP) and Kolmogorov–Arnold Network (KAN).

and GEMM benefit from deeply optimized libraries (e.g., cuDNN [4], cuBLAS [17]). In contrast, polynomial basis expansion, which uses a linear combination of basis polynomial functions to represent complex functions, still lacks a high-performance kernel library, resulting in a major bottleneck for practical KAN deployment.

To address this issue, we propose a systematic approach of GPU parallel optimization for KAN and its variants, exemplified by Chebyshev KAN (ChebyKAN). Our approach combines lookup-table (LUT) interpolation to alleviate the high cost of polynomial basis expansions, 2D tiling over inputs and outputs to improve spatiotemporal locality, two-stage reduction to mitigate atomic contention, and coefficient-layout reordering for coalesced access. This approach offers a reusable operator interface for seamless integration to prevalent deep learning frameworks, such as PyTorch. Our main contributions are summarized as follows:

- 1) **Systematic analysis of the core bottlenecks in KAN-type networks.** We identify the issues of “multi-step dependency” and “complex function calls” for high-order polynomials under GPU parallelism. Furthermore, we analyze how traditional, operator-by-operator concatenation fails to fully exploit GPU potential from both computational and memory-access perspectives.
- 2) **A general, extensible fused-kernel design paradigm.** We propose a general fused-kernel paradigm that integrates forward/backward computations with LUT-based evaluation, 2D tiling, two-stage reduction, and coefficient layout reordering, significantly reducing kernel launch overhead and atomic conflicts. This results in 1.3–2.2× speedup and 1.3–4× throughput improvement on end-to-end tasks.
- 3) **Generalization across KAN variants.** We analyze the computational characteristics of the KAN variant and demonstrate the generalization of our proposed method. The proposed fused-kernel design is independent of basis function selection, supporting KAN variants based on Chebyshev, Legendre, Fourier, etc. Additionally, the design can function as a plug-in component, enabling its seamless integration into complex model architectures such as Convolutional Networks, Graph Neural Networks, and Transformers.
- 4) **A reusable operator optimization library, PolyKAN, for polynomial/kernel approximation networks.** We implement and evaluate an open-source library, *PolyKAN*, delivering substantial training and inference speedups without accuracy loss, and providing Python APIs for better usability in domain of AI for Science. To the best of our knowledge, this is the first open-source, general GPU operator library for the polynomial-based KAN variants.

The rest of the paper overviews KAN and polynomial expansions (§2), analyzes bottlenecks and motivation (§3), details

our optimizations (§4), and presents experiments (§5) before concluding (§6).

2 Background and Related Work

2.1 Overview of KAN

As an alternative to traditional MLPs, KAN introduces a novel architecture that replaces fixed node-wise activations with learnable edge-wise univariate functions, aiming to improve both expressive efficiency and interpretability. This design is grounded in the idea that complex multivariate continuous functions can be decomposed into compositions of simpler univariate ones. The theoretical underpinning of this decomposition is the Kolmogorov-Arnold Theorem, which we briefly review below.

Theorem 2.1 (Kolmogorov-Arnold Theorem [13]). *Let $f : [0, 1]^n \rightarrow \mathbb{R}$ be an arbitrary continuous function. Then there exist continuous single-variable functions*

$\phi_0, \phi_1, \dots, \phi_{2n}$ and $\psi_{q,1}, \psi_{q,2}, \dots, \psi_{q,n}$ (for $1 \leq q \leq 2n + 1$) such that, for all $x = (x_1, x_2, \dots, x_n) \in [0, 1]^n$,

$$f(x) = \sum_{q=1}^{2n+1} \phi_q \left(\sum_{p=1}^n \psi_{q,p}(x_p) \right).$$

Based on the Kolmogorov-Arnold theorem, KAN adopts a network structure that can be broadly described as follows: for an arbitrary input vector $\mathbf{x} \in \mathbb{R}^n$, each component x_p is first mapped by a univariate function $\psi_{q,p}$, where p indexes the dimensions of \mathbf{x} and q indexes channels. The results of these mappings across all input dimensions are then summed, and the summed value is passed through another univariate function ϕ_q . Finally, the scalar outputs from all q paths are added together to produce the final output. The structure of the Kolmogorov-Arnold network is shown in Figure 2.

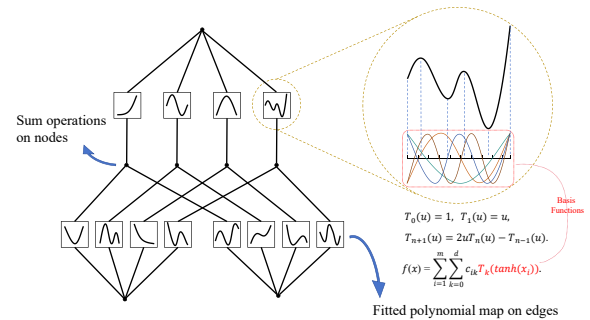


Figure 2. The structure of the Kolmogorov-Arnold network.

2.2 KAN variant: Chebyshev KAN

Chebyshev KAN [21] is a variant of KAN. The univariate basis functions are implemented with Chebyshev polynomials, replacing the conventional B-spline basis or other

activation functions. The **first computation strategy** for the Chebyshev polynomial expansion is defined as follows:

$$T_n(x) = \cos(n \arccos x), \quad x \in [-1, 1], \quad n \in \mathbb{N}. \quad (1)$$

where n denotes the order of the Chebyshev polynomial, which governs both its shape and approximation capacity. When a target function exhibits greater complexity, n typically resorts to polynomials of higher order. Since GPUs have high throughput on basic operators such as vectorized addition, subtraction, multiplication and division, the overhead of calling high-level functions such as $\cos(\cdot)$ or $\sin(\cdot)$ multiple times is much higher than addition and multiplication. Therefore, exploiting the trigonometric identity $\cos((n+1)\theta) = 2 \cos \theta \cos(n\theta) - \cos((n-1)\theta)$, investigators establish the **second computation strategy** of Chebyshev polynomial expansion by the following recurrence formula:

$$T_0(x) = 1, \quad T_1(x) = x, \quad T_{n+1}(x) = 2xT_n(x) - T_{n-1}(x). \quad (2)$$

For every input dimension p , the model evaluates the Chebyshev polynomials from T_0 up to T_{degree} . Consequently, for each dimension p , we obtain a multi-order feature set $\{T_0(x_p), T_1(x_p), \dots, T_K(x_p)\}$, where $K = \text{degree}$.

These polynomial features are subsequently combined with a set of learnable coefficients to produce the layer’s output. In the original ChebyKAN implementation, all features generated by input dimension p and polynomial order K are concatenated to form a large feature vector:

$$h = [T_0(\tilde{x}_1), T_1(\tilde{x}_1), \dots, T_K(\tilde{x}_1), T_0(\tilde{x}_2), \dots, T_K(\tilde{x}_n)]. \quad (3)$$

Let \mathbf{W} denote the learnable “coefficient matrix”, the mapping can be written as: $y = \mathbf{W} \cdot h + b$, where y denotes the output of the current layer. The network architecture of a ChebyKAN layer is shown in Figure 3.

2.3 The characteristics of the KAN variants

Numerous KAN variants share a common computational skeleton—generating multi-order basis functions for each input dimension and aggregating them with learnable coefficients. Trigonometric-based forms (e.g., Chebyshev, Fourier) leverage recurrences to propagate orders without repeated \sin/\cos evaluations. For instance, FourierKAN can exploit identities such as $\cos((k+1)x) = \cos(kx)\cos(x) - \sin(kx)\sin(x)$, thereby propagating between successive orders without invoking $\sin(kx)$ or $\cos(kx)$ for every k .

Orthogonal-polynomial and piecewise basis (e.g., Legendre, Hermite, B-splines) exhibit similar recurrence forms. Abstractly, $\alpha_k(x) B_{k+1}(x) = \beta_k(x) B_k(x) - \gamma_k B_{k-1}(x)$, leads to similar dataflows and memory-access patterns during expansion and coefficient aggregation.

It is evident that despite differences in basis form and theoretical origin, most of the KAN variants share the consistent framework of multi-order basis expansion and learnable coefficient aggregation. In the following, we take ChebyKAN

as a representative case and conduct a detailed analysis of its performance bottlenecks.

3 Performance Analysis and Motivation

In this section, we use *ChebyKAN* as a representative to analyze why KAN variant operators underutilize GPUs and motivate our optimizations. Adopting the Roofline perspective [27], we balance compute and bandwidth to identify the dominant bottlenecks. The conclusions are also applicable to other KAN variants.

3.1 Diagnosis of performance bottlenecks

Although both the trigonometric Eq. (1) and recurrence Eq. (2) formulations of Chebyshev polynomials mentioned in §2.2 are valid, the recurrence form is preferred for superior GPU efficiency. We analyze its performance bottlenecks on GPU hardware. The parameters and notations in this paper are listed in Table 1.

Table 1. Configurations of ChebyKAN.

Symbol	Meaning
B	Batch size of input data
D_{in}	Dimension of input data
D_{out}	Dimension of output data
d	Maximum order of a polynomial
λ	Bytes per element
$TILE_IN$	Thread-block tile size along Input
$TILE_OUT$	Thread-block tile size along Output
g_x	Number of input tiles, $g_x = \lceil \frac{D_{in}}{TILE_IN} \rceil$
g_y	Number of output tiles, $g_y = \lceil \frac{D_{out}}{TILE_OUT} \rceil$

As illustrated in Figure 3, the forward propagation process of ChebyKAN can be roughly divided into two steps: calculating the polynomial values of all orders and multiplying-accumulating the polynomial expansion results with the learnable coefficient matrix.

Counting fused multiply-adds conservatively as 2 FLOPs, the layer’s total work and main data movement scale as

$$T = T_{\text{expand}} + T_{\text{combine}} \approx 2BD_{in}(d + (d+1)D_{out}),$$

$$S \approx \lambda[BD_{in} + BD_{out} + 2BD_{in}(d+1) + D_{in}D_{out}(d+1)].$$

yielding arithmetic intensity:

$$I = \frac{T}{S} \approx \frac{2BD_{in}(d + (d+1)D_{out})}{\lambda[B(D_{in} + D_{out}) + 2BD_{in}(d+1) + D_{in}D_{out}(d+1)]}.$$

where I scales linearly with the batch size B and the output dimension D_{out} . Consequently, as shown in Figure 4 *ChebyKAN* operates in two distinct regimes:

- **Memory-bound** ($I < I_{\text{max}}$). Arithmetic intensity becomes too low to saturate the GPU’s compute units.

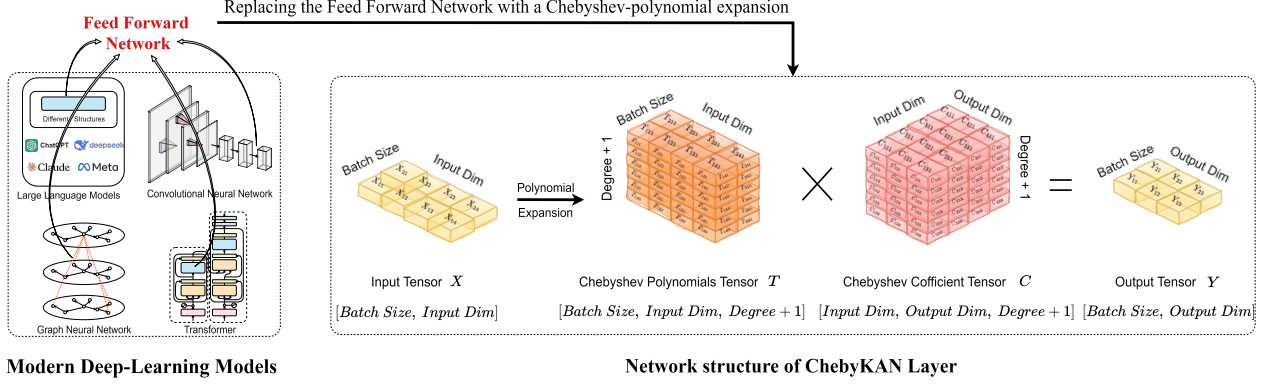


Figure 3. Replacing a conventional feed-forward layer in deep-learning models with a **ChebyKAN** layer: the input X is mapped elementwise by the Chebyshev-polynomial basis, producing the basis tensor T with entries $T_{b,j,d} = T_d(\tanh(X_{b,j}))$. The tensor T is then linearly contracted with the learnable coefficient tensor C to yield the output Y .

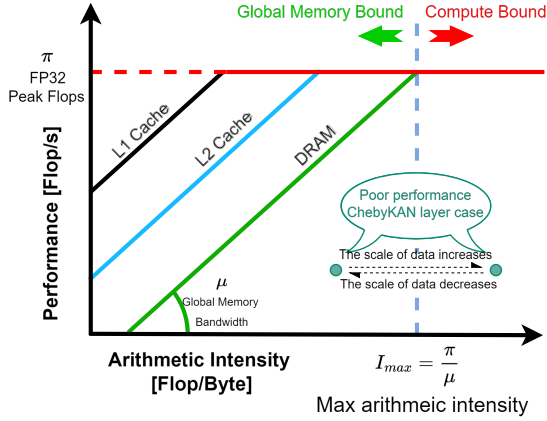


Figure 4. The roofline model of the Kolmogorov-Arnold network.

Each step of the recurrent formulation must access and update the result from the previous order. Unlike matrix multiplication, the required data cannot be pre-loaded and processed in one highly parallel pass. Additionally, if the computation of small segments is not properly batched within the same block/warp, the kernel incurs frequent global-memory accesses or redundant data loads.

- **Compute-bound** ($I \geq I_{\max}$). Scaling both B and D_{out} pushes the arithmetic intensity I past the ridge point. Yet the loop-carried dependencies in the recurrent basis-function generator restrict instruction-level parallelism. Additionally, the enlarged set of polynomials and coefficients inflate the per-thread register footprint, thereby lowering Streaming Multiprocessor(SM) occupancy.

Therefore, our optimization strategy focuses on cutting global-memory traffic and maximizing in-block data reuse. These measures simultaneously raise arithmetic intensity in memory-bound case and improve compute utilization when the workload crosses into the compute-bound regime.

3.2 Related GPU optimization work

From the viewpoint of classical high-performance computing (HPC) and numerical analysis, both industry and academia have already undertaken extensive optimization of **trigonometric function** and **polynomial recurrence**. Libraries such as Intel Vector Math Library (VML) [10], the CUDA math API [18], and other specialized vector-function packages offer hand-tuned vectorization, SIMD/SIMT parallelism, and approximation techniques that greatly reduce the latency of single-point or small-batch function calls. For the aggregation phase, dense GEMM libraries such as cuBLAS and CUTLASS attain near-peak hardware throughput. Some recent work, such as FusedFourierKAN [8], has optimized the performance of the KAN variant based on Fourier polynomial from an overall operator perspective.

However, these libraries perform well at their respective micro-kernels, with only particular execution stages optimized. Traditional vector math libraries usually only map functions like $\cos(x)$ and $\exp(x)$ to vectorized implementations, and do not fully optimize for the large number of intermediate steps that exist in multi-order recurrence. They also lack a design that fuses these basis function computations with the subsequent multiply-accumulate of learnable coefficients. Although FusedFourierKAN attempts to fill this gap, it relies on simple kernel fusion, yielding limited performance gains, and its design is tightly coupled to the Fourier basis, which hinders extension to other polynomial bases. This motivates the general optimization pipeline proposed

in the present work. To our knowledge, our proposed solution first provides a unified, variant-agnostic acceleration framework for KAN-style operators.

4 Methodology

4.1 Overview

To accelerate both forward and backward propagation of KAN operators (e.g., CHEBYKAN, LEGENDREKAN) on modern GPUs, we design a generic optimization pipeline. Its guiding principle is to maximize parallelism while minimizing memory pressure without sacrificing support for different polynomial bases. The overall design is shown in Figure 5. The proposed pipeline consists of four orthogonal methods:

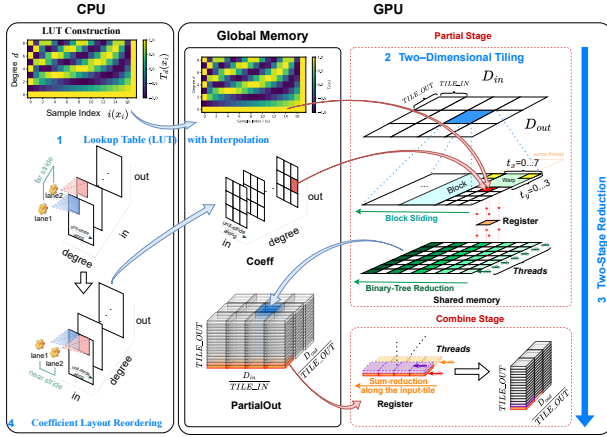


Figure 5. The overall design of the KAN variant acceleration.

- 1. Lookup Table (LUT) with Interpolation.** The basis functions of many polynomials (e.g., Chebyshev, Legendre) can be pre-computed offline and stored in a large LUT [1]. At run time, we obtain approximations by linear (or higher-order) interpolation, eliminating expensive trigonometric evaluations or recurrence formulations. Our implementation allocates the LUT in global memory, so as to meet high-precision requirements while alleviating constant-memory capacity constraints.
- 2. 2D Tiling.** We adopt a 2D tiling strategy by simultaneously partitioning the input and output dimensions into rectangular blocks of configurable size. Each GPU thread block is assigned to process a single tile, performing the corresponding multiply-accumulate operations locally. This design improves data access spatial locality, which enhances cache reuse and enables fine-grained parallelism across both dimensions.
- 3. Two-Stage Reduction (Partial + Combine).** We adopt a two-stage scheme to avoid large-scale atomicAdd operations on the same output location which cause severe resource contentions. In the *Partial* stage, each tile accumulates its partial sum in shared memory. The

Combine stage then merges partial results from different tiles into the final output, reducing atomic contention and write-conflict overhead.

- 4. Coefficient Layout Reordering.** The original coefficient tensor is usually stored as $[inputdim, outputdim, degree + 1]$, which leads to large access strides inside the kernel. We reorder it to $[degree + 1, outputdim, inputdim]$, enabling contiguous memory accesses and higher bandwidth utilization.

By applying the four key optimization steps described above, the proposed implementation significantly reduces the number of explicit function calls, bandwidth waste, and atomic collisions in both forward and backward propagation.

4.2 Polynomial Operators Acceleration via LUT

Many polynomial basis functions employed in the KAN variants, such as Chebyshev, Legendre, and Hermite, share two universal properties:

- **Domain normalization to $[-1, 1]$.** Each basis is either intrinsically defined on the interval $[-1, 1]$ or can be mapped to that interval by a simple normalization step. For example, the input x in ChebyKAN can be transformed by $\tanh(\cdot)$ so as to ensure that $x \in [-1, 1]$.
- **Offline discretization and storage.** The polynomial function $p_d(x)$ of any KAN variant attains a deterministic value for fixed $degree$ and x . Therefore, we can sample $p_d(x)$ on the CPU over the interval $[-1, 1]$ with an appropriate step size, compute the results iteratively, and store them in a LUT.

These properties enable the *LUT-interpolation* strategy and demonstrate its *generality*: regardless of the particular polynomial basis, once the function can be discretized over $[-1, 1]$ and a LUT built for the required $degree$, the same strategy is always applicable.

4.2.1 Offline construction of LUT.

We first construct the LUT on the CPU. For a prescribed maximum $degree$ we choose a table size LUT_SIZE and discretize the interval $[-1, 1]$ with the uniform step: $\Delta = \frac{2}{LUT_SIZE-1}$.

At each grid point $x_i = -1 + i \Delta$ ($i = 0, 1, \dots, LUT_SIZE-1$) we evaluate the sequence $T_0(x_i), T_1(x_i), \dots, T_{degree}(x_i)$ by applying the recurrence in Eq. (2) once, and write the results into a two-dimensional array LUT . $LUT[d, i]$ stores the value of the d -th basis function at the i -th sample. For other KAN variants, one merely replaces the Chebyshev recurrence with the corresponding polynomial relation, leaving the subsequent interpolation logic unchanged.

After LUT has been generated on the CPU, it is uploaded to the GPU. While storing the table in read-only on-chip memory could reduce access latency, its size exceeds the available capacity. Consequently, the LUT is stored in global memory, providing every thread in the subsequent kernels with read-only access to the precomputed polynomial values.

4.2.2 Online interpolation from LUT.

Once a GPU thread receives an input value $x \in [-1, 1]$, it approximates $T_d(x)$ from the lookup table in two steps: (i) *calculate its normalized position in the interval $[-1, 1]$ based on x : $pos = \frac{x+1}{2}(LUT_SIZE - 1)$* ; (ii) *perform linear interpolation between the two neighbouring samples whose indices are $\lfloor pos \rfloor$ and $\lfloor pos \rfloor + 1$.*

This procedure produces a close approximation to $T_d(x)$ without invoking run-time trigonometric functions or the recurrence relation.

Linear interpolation suffices for most applications: the grid spacing $\Delta = 2/(LUT_SIZE - 1)$ is small with a large LUT_SIZE , rendering the interpolation error negligible over the interval. Higher-order schemes (quadratic or cubic) could further reduce error but at the cost of additional arithmetic. Therefore, the linear variant strikes a favorable balance between simplicity and efficiency.

In both forward and backward propagation, both polynomial values and their derivatives can be obtained directly from the LUT. For the derivative, we can approximate $\frac{d}{dx}T_d(x)$ by a finite difference between neighbouring table entries, or store the pre-computed differences as an auxiliary LUT. In this work, using the Chebyshev basis as an example, the backward gradient is computed from either T_{approx} or the difference of adjacent samples, avoiding explicit evaluations of the analytic derivative. §4.3 revisits this strategy when discussing backward propagation 2.

4.3 Parallelism of 2D tiling across the input and output dimensions

The computational workload scales with $D_{in} \cdot D_{out}$. One-dimensional parallelization over the batch axis forces warps to stride long distances in either dimension, leading to non-coalesced memory traffic. We therefore adopt **2D tiling**: partition input into $TILE_IN$ and output into $TILE_OUT$. Each CUDA block is assigned a $TILE_IN \times TILE_OUT$ sub-matrix, but it processes it using a specialized “output-aligned” warp strategy. This design (i) improves spatial locality for both coefficient and LUT accesses, (ii) confines atomicAdd operations to localized output regions, reducing contention, and (iii) generates a larger set of load-balanced blocks, enabling the scheduler to saturate all SMs more effectively.

Block-grid configuration and thread mapping. Let $grid = (g_x, g_y, B)$, where $g_x = \lceil \frac{D_{in}}{TILE_IN} \rceil$ and $g_y = \lceil \frac{D_{out}}{TILE_OUT} \rceil$. Critically, we set the block dimensions to $block = (BLOCK_DIM_X, BLOCK_DIM_Y)$, where $BLOCK_DIM_Y$ is typically 32 (a full warp) and $BLOCK_DIM_X$ is a smaller value (e.g., 8). A block (tileI, tileO, b) processes the sub-tile (Δ_i, Δ_o) using a different thread mapping:

- The thread’s y index, t_y , maps directly to the output dimension: $o = \Delta_o \cdot start + t_y$. This aligns a full warp (32 threads) along the output dimension.

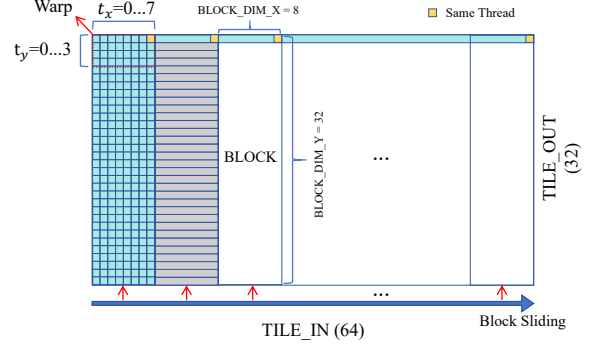


Figure 6. Visualization of the output-aligned 2D tiling strategy. A single BLOCK (8×32 threads) maps its t_y index 1:1 to the $TILE_OUT$ dimension. A hardware Warp is an 8×4 tile. The “Same Thread” (yellow) iterates across the $TILE_IN$ dimension with a stride of $BLOCK_DIM_X (8)$.

- The thread’s x index, t_x , maps to the *offset* of the input dimension j .

To cover the entire $TILE_IN$ range (e.g., 64), each thread is assigned multiple j indices to process. This iteration uses the thread’s t_x index as an initial offset and a stride of $BLOCK_DIM_X$. Figure 6 provides a visual representation of this block configuration and iterative mapping.

This *output-aligned* configuration is a deliberate choice to resolve a critical performance bottleneck in the LUT access. This bottleneck arises from a fundamental trade-off between the ideal access patterns for the LUT and Coeff tensors:

- **Ideal LUT Access (1-way Broadcast):** To minimize LUT memory divergence, a warp requires as few distinct j values as possible. The ideal scenario provides **1 distinct j value** and allows for a perfect 1-way broadcast from the LUT.
- **Ideal Coeff Access (32-way Coalescing):** To maximize Coeff coalescing, a warp requires many consecutive j values. The ideal scenario provides **32 distinct j values** for a perfect 32-way coalesced access.

These two ideal scenarios are mutually exclusive. A naive tiling strategy (e.g., a 64×16 block mapping $t_x \rightarrow j$) would result in a hardware warp containing 32 distinct j values. Since the LUT index idx is calculated from j , this naive mapping causes a severe **32-way memory scatter**.

Our $(8, 32)$ block design is specifically chosen to be a trade-off. A warp in this configuration is an 8×4 tile, containing only **8 distinct j values** (one for each t_x). This design reduces the LUT memory bottleneck to a much more manageable **8-way scatter** when accessing the LUT.

Coefficient/LUT memory layout and coalesced accesses. As established in the previous section, our $(8, 32)$ block configuration is designed to solve the primary bottleneck of LUT memory by reducing it to an 8-way scatter. This

block-level decision, in turn, dictates the optimal memory layout for the *Coeff* tensor.

Given this $(8, 32)$ block, a hardware warp is an 8×4 tile, and its 8 *consecutive* threads (e.g., $ty=0, tx=0..7$) are mapped to 8 different j indices. We must choose a layout that makes these 8 accesses efficient.

Therefore, we reorder the coefficient tensor to the $[d, o, j]$ layout, where j is the **innermost dimension**. With this layout, the same 8 consecutive threads now access contiguous memory addresses. Therefore, the hardware executes this as a single, efficient **8-way coalesced read**. This same coalescing benefit applies to the `atomicAdd` operations during the backward pass. This strategy, detailed further in §4.5.

The forward and backward propagation process. In the forward propagation, each sub-block carries out the multiply-accumulate of polynomial values over its designated Δ_i and Δ_o . The forward propagation can be summarized by Algorithm 1, which reflects the new outer iterative loop over the j dimension. Each thread evaluates Chebyshev terms via `LookupCheby` on $\tanh(x_{b,j})$ (§4.2) and accumulates over the degree in registers, returning the vector $T_0(x_i), T_1(x_i), \dots, T_{degree}(x_i)$.

During the backward propagation, we apply the same output-aligned 2D tiling strategy to the output gradient $\partial \mathcal{L} / \partial y$. Within each (Δ_i, Δ_o) sub-tile, the gradients with respect to both the coefficients and the inputs are computed in batch. The corresponding pseudocode is presented as Algorithm 2.

4.4 Two-Stage Reduction

When either the data dimensions or the batch size are large, each CUDA block must accumulate a portion of the output (or its gradient) within a single kernel launch. Even with 2D tiling along the input and output axes, writing directly to the global output or the gradient array still incurs three major drawbacks:

- **Atomic contention.** Whenever multiple blocks update the same batch item or the same output element, a large number of `atomicAdd` operations are inevitable and quickly become a performance bottleneck.
- **Write-after-read latency.** Since atomic updates are serialized by the hardware, repeated atomic writes to the same address within one kernel stall the instruction pipeline and introduce extra latency.
- **Superfluous atomic overhead.** Atomic writes are significantly more expensive than ordinary stores. Aggregating partial sums in an intermediate buffer and performing a single consolidated write-back would cut down the total number of atomic operations.

To mitigate these issues we introduce a **two-stage reduction** (*Partial* + *Combine*). In the *Partial* stage, each block stores its results in a private, conflict-free buffer. Subsequently, in the *Combine* stage, these buffers are merged into

Algorithm 1: Forward propagation (Partial Stage) with output-aligned 2D tiling and $[d, o, j]$ layout.

Input: $X \in \mathbb{R}^{B \times D_{in}}, Coeff \in \mathbb{R}^{(degree+1) \times D_{out} \times D_{in}}, LUT \in \mathbb{R}^{(degree+1) \times LUT_SIZE}, tile_{in}, tile_{out}, BLOCK_DIM_X}$
Output: $partialOut \in \mathbb{R}^{(g_x \times g_y \times B \times tile_{out})}$

```

1 for b ← 0 to B − 1 in parallel do
2   for tileI ← 0 to  $\lceil D_{in}/tile_{in} \rceil - 1$  in parallel do
3     for tileO ← 0 to  $\lceil D_{out}/tile_{out} \rceil - 1$  in parallel do
4        $in_{start} \leftarrow tileI \times tile_{in}$ 
5        $in_{end} \leftarrow \min(in_{start} + tile_{in}, D_{in})$ 
6        $out_{start} \leftarrow tileO \times tile_{out}$ 
7        $out_{end} \leftarrow \min(out_{start} + tile_{out}, D_{out})$ 
8        $g_x \leftarrow \lceil D_{in}/tile_{in} \rceil$ 
9        $smem[BLOCK\_DIM\_Y][BLOCK\_DIM\_X]$ 
10      for  $(t_x, t_y) \leftarrow (0..BLOCK\_DIM\_X - 1, 0..BLOCK\_DIM\_Y - 1)$  in parallel do
11         $out \leftarrow out_{start} + t_y$ 
12         $sum\_total \leftarrow 0$ 
13        if  $out < out_{end}$  AND  $b < B$  then
14          for j ←  $in_{start} + t_x$  to  $in_{end} - 1$  step  $BLOCK\_DIM\_X$  do
15             $x \leftarrow \tanh(X[b, j])$ 
16             $T_{approx} \leftarrow \text{LookupCheby}(LUT, x, degree)$ 
17             $sum\_total \leftarrow sum\_total + \text{dot}(Coeff[:, out, j], T_{approx})$ 
18           $smem[t_y, t_x] \leftarrow sum\_total$ 
19          WaitAndReduceOverX( $smem[t_y, t_x]$ )
20          if  $t_x = 0$  AND  $out < out_{end}$  AND  $b < B$  then
21             $gIdx \leftarrow (tileO \times g_x + tileI) \times B \times tile_{out} + b \times tile_{out} + t_y$ 
22             $partialOut[gIdx] \leftarrow smem[t_y, 0]$ 

```

the global output, converting many fine-grained atomic updates into a small, well-controlled batch of writes.

4.4.1 Partial and Combine stages.

In forward propagation, each thread block writes its partial sum to device-global workspace buffer `PartialOut` instead of issuing global atomics. Every sub-block created by the 2D tiling scheme owns a dedicated segment (denoted by `subBlockID`) inside this buffer, preventing write conflicts between blocks.

Algorithm 2: Backward propagation with output-aligned 2D tiling and $[d, o, j]$ layout.

Input: $X \in \mathbb{R}^{B \times D_{in}}$, $Coeff \in \mathbb{R}^{(degree+1) \times D_{out} \times D_{in}}$,
 $LUT \in \mathbb{R}^{(degree+1) \times LUT_SIZE}$,
 $tile_{in}, tile_{out}, BLOCK_DIM_X$

Output: $coeff_grad \in \mathbb{R}^{(degree+1) \times D_{out} \times D_{in}}$,
 $x_grad \in \mathbb{R}^{B \times D_{in}}$

// The following is executed by each block
 $(tileI, tileO, b)$ in parallel

```

1  $in_{start} \leftarrow tileI \times tile_{in}$ 
2  $in_{end} \leftarrow \min(in_{start} + tile_{in}, D_{in})$ 
3  $out_{start} \leftarrow tileO \times tile_{out}$ 
4  $out_{end} \leftarrow \min(out_{start} + tile_{out}, D_{out})$ 
5  $smemX[BLOCK\_DIM\_X][BLOCK\_DIM\_Y]$ 
   // Shared mem for  $x\_grad$ 
   // Each thread  $(t_x, t_y)$  executes in parallel
6 if  $b < B$  then
7   for  $j \leftarrow in_{start} + t_x$  to  $in_{end} - 1$  step
      $BLOCK\_DIM\_X$  do
8      $out \leftarrow out_{start} + t_y$ 
9      $x\_grad\_partial \leftarrow 0$ 
10    if  $out < out_{end}$  then
11       $g_o \leftarrow dY[b, out]$ 
12       $x \leftarrow \tanh(X[b, j])$ 
13       $(T_{approx}, dTdx) \leftarrow$ 
        LookupChebyAndDiff( $LUT, x, degree$ )
14       $sum\_dx \leftarrow 0$ 
15      for  $d \leftarrow 0$  to  $degree$  do
16        atomicAdd( $coeff\_grad[d, out, j], g_o \times$ 
           $T_{approx}[d]$ )
17      for  $d \leftarrow 1$  to  $degree$  do
18         $c\_val \leftarrow Coeff[d, out, j]$ 
19         $sum\_dx \leftarrow$ 
           $sum\_dx + g_o \times c\_val \times dTdx[d]$ 
20       $x\_grad\_partial \leftarrow sum\_dx$ 
21     $smemX[t_x, t_y] \leftarrow x\_grad\_partial$ 
22     $final\_x\_sum \leftarrow$ 
      BlockReduceOverY( $smemX[t_x, :]$ )
      // Syncs & sums  $smemX[t_x][0..31]$ 
23    if  $t_y = 0$  then
24      atomicAdd( $x\_grad[b, j], final\_x\_sum$ )
25    SyncBlock()
      // Wait for all threads before next j

```

After completion of the *Partial* stage, the partial sums generated by all sub-blocks reside in *PartialOut*. The subsequent **Combine** stage merges these values. This process is

typically completed within a single kernel launch, obtaining the final output y .

Since the values can be accumulated sequentially while iterating over the subBlockIDs, the amount of write contention is greatly reduced at this stage. If a fully parallel merge is desired, hierarchical or tree-based reduction schemes can be employed to balance efficiency against implementation complexity.

4.4.2 Performance benefit analysis.

Compared to a single-kernel direct write-back, the two-stage reduction maintains a unique-writer invariant for every intermediate and final location, thus eliminating all global atomics in forward. The Combine stage performs ordinary streaming loads and a single store per (b, out) . For gradients, we retain a minimal set of atomics: (i) coefficient gradient aggregates across batches on the same (d, j, out) ; (ii) input gradient uses per-block reduction along out , followed by a single atomic add per (b, j) to merge contributions across g_y output tiles. This reduces atomics from $BD_{in}D_{out}$ to $BD_{in}g_y$.

Atomic update count (forward). A block-reduction + atomic-write baseline performs $N_{atomic, fwd}^{base} = B \cdot D_{out} \cdot g_x$ atomic updates. Our two-stage reduction eliminates them: $N_{atomic, fwd}^{ours} = 0$.

Bandwidth and temporary footprint. Two-stage introduces a streaming intermediate $S_{partial} \approx \lambda B D_{out} g_x$ bytes and extra I/O $2 \times S_{partial}$ (write+read). Two-stage is beneficial when $g_x c_a \gtrsim g_x (c_r + c_w) + c_w$, i.e., when the per-atomic cost c_a dominates normal read cost c_r and write costs c_w .

Backward x -gradient. A naive design would require $B \cdot D_{in} \cdot D_{out}$ atomics. With intra-block reduction along out , ours reduces it to $N_{atomic, bwd-x}^{ours} = B \cdot D_{in} \cdot g_y$, avoiding fine-grained atomic contention. A further two-stage process would remove atomics at the cost of an extra buffer of $\lambda B D_{in} g_y$ bytes and an additional launch, which is not cost-effective in our methodology.

4.5 Coefficient layout reordering

In typical implementations of KAN networks, the polynomial coefficients are stored for every input dimension j and output dimension o . When the tensor is kept in its default three-dimensional layout, GPU threads must access elements with excessively large strides, which in turn diminishes both coalesced memory throughput and cache efficiency.

4.5.1 Original layout and memory-access pattern.

In the baseline implementation, the coefficients are stored in the index order (j, o, d) , i.e. as a three-dimensional array $coeff[D_{in}][D_{out}][degree+1]$. Although this layout is intuitive for CPU code — one loops over every input index j and output index out before selecting the desired degree d , it leads to sub-optimal access patterns on the GPU. Under a 2D tiling scheme in which a thread block sweeps across

$D_{\text{in}} \times D_{\text{out}}$ and then iterates over d , two contrasting stride behaviours emerge:

- When a *single* thread reads successive polynomial orders $\text{coeff}[j, o, d]$, the stride along the d -dimension is small and cache-friendly.
- However, if threads in the same warp handle neighbouring (j, o) pairs, their memory accesses are scattered across the first two dimensions of the array, producing non-contiguous addresses and poor coalescing efficiency.

4.5.2 Reordering the coefficient to the layout $[d, o, j]$.

To solve the access pattern problem, we reorder the coefficient tensor as $\text{coeff_rearr}[d, o, j]$. This layout is not chosen in isolation; it is specifically designed to work in synergy with the $(8, 32)$ *output-aligned* block strategy.

As established in §4.3, our $(8, 32)$ block is designed to have 8 distinct j values within a warp (from $t_x = 0..7$) to solve the LUT bottleneck. With this block shape, a hardware warp is an 8×4 tile, and its 8 *consecutive* hardware threads (e.g., $ty=0, tx=0..7$) are mapped to 8 different but consecutive j indices. We must choose a layout that makes these 8 simultaneous accesses efficient. Therefore, we reorder the coefficient tensor to the $[d, o, j]$ layout, where j is the **innermost dimension**. Since these threads access contiguous memory addresses, the hardware executes this as a single, efficient **8-way coalesced read**.

Additionally, this layout benefits for both forward and backward propagations. Forward propagation reads $\text{coeff}[d, o, j]$ with coalesced loads. Backward propagation writes to $\partial \mathcal{L} / \partial \text{coeff}[d, o, j]$, which benefits equally from **coalesced atomicAdd** operations, significantly reducing atomic contention on the memory bus.

When D_{in} and D_{out} are large, this new layout, combined with our specific tiling strategy, raises effective bandwidth and hence throughput on identical hardware.

Since this method relies only on the enumerability of the $\text{degree} + 1$ axis, it is applicable to Legendre, Hermite, and other KAN variants.

5 Experiment

This section evaluates the practical effectiveness of the ChebyKAN optimizations. The study adopts a macro-to-micro protocol. Firstly, for three representative end-to-end workloads, we measure epoch-level training and inference latency as well as sample throughput for seven kernel versions, including both baselines, on an NVIDIA A100 GPU. Second, we isolate a single ChebyKAN layer under the same three input-output-degree configurations and record forward and backward latency to analyse operator-level scalability. Finally, we construct a roofline model to quantify how the proposed methodology schemes mitigate micro-architectural bottlenecks.

Importantly, our goal is to evaluate the effectiveness of our proposed KAN operator as an MLP replacement. Thus, we choose ChebyKAN-dominant models to highlight the operator’s performance gains. This approach is crucial for isolating the acceleration of our fused kernels, ensuring that the measured speedups are not confounded by other complex operators (e.g., attention mechanisms, graph convolutions or PDE residual calculations) present in larger, state-of-the-art architectures. Our ultimate aim is to validate that our optimized operator can serve as an efficient, plug-in replacement for Linear layers, enabling future work to reconstruct existing deep learning models with KAN variants.

5.1 Hardware & Software Environment

All experiments are conducted on a single NVIDIA A100-SXM4-40 GB GPU which sustains theoretical peaks of 19.5 TFLOPS FP32.

The software stack comprises Ubuntu 22.04 LTS (kernel 5.15), CUDA 12.6. High-level execution relies on PyTorch 2.2.0+cu126. Micro-architectural data are gathered with Nsight Compute 2024.1 in kernel performance-replay mode. Timing is obtained with CUDA events placed around each kernel, synchronising the stream before and after measurement; data-loader overheads are excluded.

5.2 Workloads and Baselines

5.2.1 Benchmark Suite.

Our benchmark suite comprises three distinct datasets, with key parameters summarized in Table 2. For **Google Speech Commands v2** [26], each sample is a one-second utterance intended for single-word classification. The **VoiceBank-DEMAND** [24] dataset is constructed by mixing clean utterances from the VoiceBank corpus with various environmental noise recordings from the DEMAND database. It is repurposed for an acoustic-scene classification task. For the **Kaggle House-Prices** [12] regression task, the model predicts the target market price from 79 raw features. The input is either zero-padded or truncated to a uniform dimension.

These three tasks jointly cover audio classification, speech enhancement, and structured-data regression, and span operator widths from 40 to 1024, providing a representative test bed for assessing ChebyKAN performance.

5.2.2 Baseline Implementations.

Seven kernels are evaluated. All kernels are functionally identical (FP32 forward, FP32 gradients). The description of each method is given in Table 3.

Baseline-1 evaluates Chebyshev basis via the trigonometric form. Baseline-2 (cuBLAS) [22] constructs Chebyshev basis via the recurrence form and employs the stock PyTorch implementation, which internally dispatches dense GEMM calls to NVIDIA’s cuBLAS library. CuBLAS is widely regarded as the industry-standard, vendor-tuned kernel for general-purpose matrix multiplication on GPUs. Specifically, PyTorch

Table 2. Benchmark Suite Summary

Dataset	Description	Layer Widths	Degree	Batch Size
Google Speech Commands v2	105,872 utterances, 35 labels	40 \rightarrow 256 \rightarrow 256 \rightarrow 12	8	128
VoiceBank-DEMAND	28 speakers, 13 noises, 13 categories	257 \rightarrow 512 \rightarrow 512 \rightarrow 13	15	64
Kaggle House-Prices	1460 properties, 79 raw features	512 \rightarrow 1024 \rightarrow 1024 \rightarrow 1	24	32

Table 3. Kernel version of baselines and our KAN implementations.

Kernel version	Incremental Optimization Steps	Primary Bottleneck Solved
Baseline-1(BL1)	Direct evaluation of acos/cos .	(N/A - Slowest baseline)
Baseline-2(BL2)	PyTorch + cuBLAS [17].	(N/A - Strong baseline)
V1	Chebyshev recurrence ($T_n = 2xT_{n-1} - T_{n-2}$)	Replaces acos/cos calls.
V2	V1 + Opt 1: LUT Interpolation.	Eliminates recurrence.
V3	V2 + Opt 2: Output-Aligned 2D Tiling.	Mitigates 32-way LUT scatter (reduces to 8-way).
V4	V3 + Opt 3: Two-Stage Reduction.	Solves forward-pass atomic contention.
V5 (PolyKAN)	V4 + Opt 4: Layout Reordering.	Solves 8-way Coeff stride (enables coalescing).

2.2 decomposes the layer into a Triton kernel [23] that materializes Chebyshev basis and a GEMM core executed by cuBLAS [17]. For small tensors Triton fuses both stages into one kernel. Baseline2 represents the most efficient implementation currently used by ChebyKAN. Versions V0 \rightarrow V5 are evaluated cumulatively. **Each version inherits all preceding optimizations.**

5.3 End-to-End Evaluation

To quantify the user-perceived benefit of the proposed optimizations, we measure the end-to-end training and inference cost of all seven kernel versions on three workloads. As the performance of Baseline-1 (BL1) is orders of magnitude worse than the other kernel versions, including it in Figure 7 would severely distort the y-axis and make the results of the other versions difficult to discern. Therefore, we report the results for BL1 separately. The total single-epoch latency for BL1 on the Speech Commands, VoiceBank, and House-Prices tasks are 1798ms, 7193ms, and 3127ms, respectively. Figure 7 consolidates, for each workload, the wall-clock time of a single epoch for the remaining kernel versions into two components: forward propagation and backward propagation on the training split.

From Baseline-1 to Baseline-2, replacing the conventional CUDA kernels with a cuBLAS-based reference already reduces epoch time by 7–11 \times . Our optimization version V5 shortens the epoch by 1.3–2.2 \times compared with Baseline-2.

As detailed in Table 4, V5 demonstrates significant throughput improvements across all tasks. For the Google Speech Commands v2 workload, V5 achieves an overall speed-up of 14.8 \times relative to Baseline-1 and 3.9 \times over Baseline-2. For the VoiceBank-DEMAND dataset, V5 outperforms Baseline-1 and Baseline-2 by factors of 15 \times and 2.1 \times , respectively. On

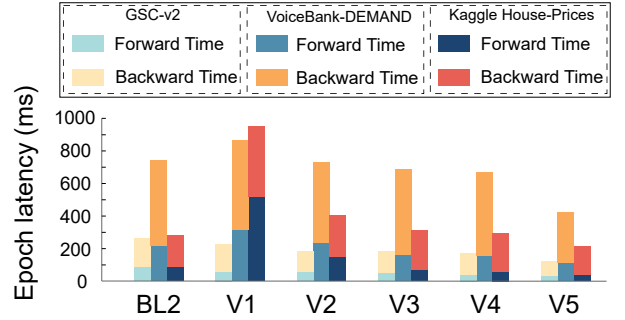


Figure 7. Epoch latency of different versions on three benchmarks.

the House-Prices regression task, V5 yields a 12.6 \times gain compared to the initial implementation and a 1.3 \times improvement over the cuBLAS-optimized baseline.

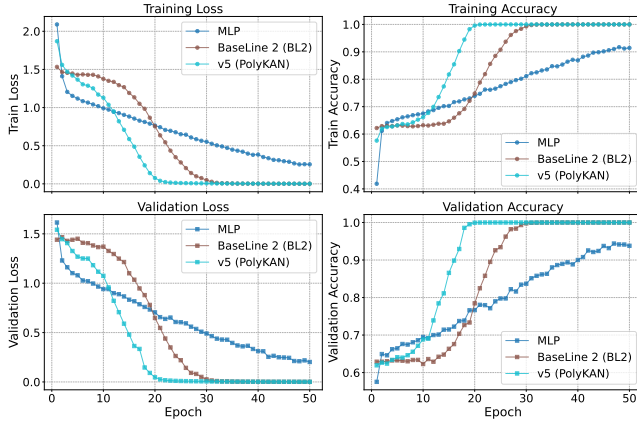
5.4 Numerical Fidelity and Convergence Speed Evaluation

A primary concern with replacing an exact mathematical formulation (i.e., Chebyshev recurrence) with an LUT-based interpolation is the potential loss of numerical fidelity. In our end-to-end evaluation, we therefore explicitly compared the final model accuracy of our optimized **V5 (PolyKAN)** operator against the **Baseline-2 (BL2)** implementation and MLP implementation. We conducted this analysis on the Speech Commands and Kaggle House Prices tasks. We omitted the VoiceBank-DEMAND task from this comparison, as its simplicity led all models to achieve 100% accuracy within the first few epochs, offering no meaningful differentiation.

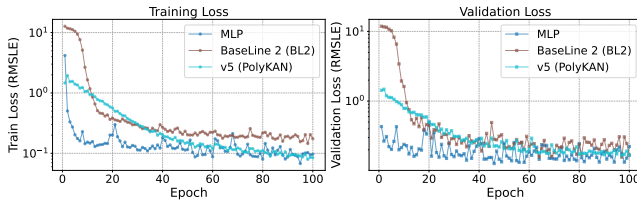
The results, presented in Figure 8a and 8b, confirm that our interpolation-based optimizations preserve numerical

fidelity. On the House Prices task, PolyKAN achieves a final validation RMSLE comparable to or better than both MLP and BL2. On Speech Commands task, PolyKAN not only matches but ultimately outperforms the BL2 baseline, achieving a higher convergence rate.

We attribute this accelerated convergence to the fundamental difference in gradient computation. Baseline-2 (Recurrence) uses PyTorch’s autograd on the exact recurrence formula, which produces a complex and high-frequency “jagged” gradient landscape for high-degree polynomials. Conversely, our V5 (PolyKAN) kernel computes an *approximate, piecewise-constant* gradient derived from the finite difference between LUT sample points ($(t_R - t_L) / \text{step}$). This “smoother” gradient acts as an implicit regularizer, allowing the Adam optimizer to find a more stable and rapid descent path. Our fused operator thus provides a dual benefit: not only is each training step significantly faster, but fewer steps are required to reach the optimal model accuracy.



(a) Training and validation loss/accuracy on the GSC-v2 task.



(b) Training and validation loss (RMSLE) on the Kaggle House Price task.

Figure 8. Comparison of convergence behavior of V5 (PolyKAN) and the recurrence-based BL2 on (a) the GSC-v2 task and (b) the Kaggle House Price task.

5.5 Operator-Level Performance Analysis

Table 5 contrasts the layer latency of the seven implementations on A100 GPU. We benchmark three precisely defined tensor configurations so that the micro-benchmarks mirror the shapes encountered in the end-to-end experiments:

Table 4. Throughput (samples/s) across three kernels.

Workload	Baseline-1	Baseline-2	V5
Speech Commands	5538	21029	82030
VoiceBank	1451	10281	21850
House-Price	396	3721	5000

- **Config. 1:** a mini-batch of 128 samples with 40 features transformed to 256 features, degree 8;
- **Config. 2:** a mini-batch of 64 samples with 256 features transformed to 512 features, degree 15;
- **Config. 3:** a mini-batch of 32 samples with 512 features transformed to 1024 features, degree 24.

These three shapes span the three regimes of our workloads, ensuring that layer-level measurements are directly comparable to the end-to-end results.

V5 (PolyKAN) achieves its most dramatic speedup in the small-scale configuration (Config. 1), delivering a 12.5 \times reduction in total latency over BL2. As problem size and computational density increase (Config. 2 and 3), V5 maintains a robust 1.4–3.9 \times speedup over BL2. Figure 9 maps representative kernels onto the roofline model, revealing a coherent migration of the performance bottleneck that validates our strategy. The multi-level roofline plot confirms that PolyKAN attains a superior balance of arithmetic intensity and hardware utilization. By tailoring thread-level parallelism to each stage’s resource mix, PolyKAN sustains consistently high GPU activity.

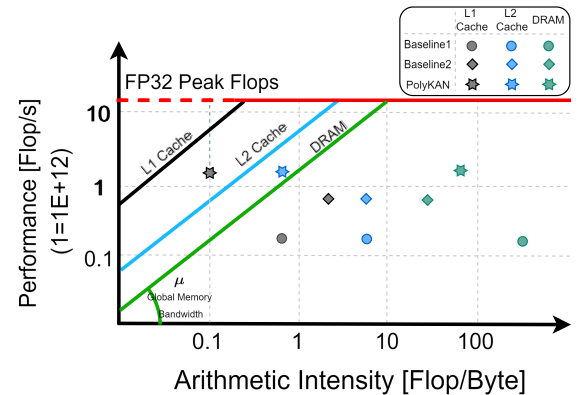


Figure 9. Multi-Level Roofline Analysis (L1, L2, DRAM) of Baseline Implementations vs. PolyKAN.

5.6 General Applicability Evaluation

To assess generalization, we apply our acceleration techniques to FourierKAN and benchmark it against the state-of-the-art FusedFourierKAN [8] accelerator. On an A100 GPU, we measured throughput and end-to-end latency on

Table 5. Operator-level latency single layer’s forward and backward pass, measured on an NVIDIA A100 GPU.

Kernel Version	Config. 1 (Speech-like)			Config. 2 (VoiceBank-like)			Config. 3 (HousePrice-like)		
	Fwd (ms)	Bwd (ms)	Sum (ms)	Fwd (ms)	Bwd (ms)	Sum (ms)	Fwd (ms)	Bwd (ms)	Sum (ms)
Config. (B, D _{in} , D _{out} , d)	(128, 40, 256, 8)			(64, 256, 512, 15)			(32, 512, 1024, 24)		
Baseline-1 (BL1)	1.301	2.577	3.878	13.881	22.359	36.240	33.541	66.806	100.347
Baseline-2 (BL2)	0.526	1.588	2.114	1.180	4.186	5.366	2.032	6.389	8.421
V1	0.181	1.026	1.207	3.683	4.378	8.061	29.108	19.031	48.139
V2	0.185	0.414	0.599	1.659	3.003	4.662	4.666	10.971	15.637
V3	0.064	0.450	0.514	0.791	3.311	4.102	1.985	9.695	11.680
V4	0.053	0.450	0.503	0.652	3.179	3.831	1.706	9.699	11.405
V5 (PolyKAN)	0.046	0.123	0.169	0.376	1.006	1.382	1.580	4.500	6.080

Table 6. Performance Comparison: FusedFourierKAN vs. OurFourierKAN on Speech Commands Dataset.

Model	Forward Latency (ms/batch)	Backward Latency (ms/batch)	Throughput (samples/s)
FusedFourierKAN	2.76	9.63	10327
OurFourierKAN	0.52	1.84	54222

the Speech Commands task, with results presented in Table 6.

Relative to FusedFourierKAN, our general optimization methods achieved a 5× increase in throughput while simultaneously reducing latency by a factor of 5. In addition to ChebyKAN and FourierKAN, applying the same optimization methodology to other KAN variants, such as LegendreKAN, HermiteKAN, also delivers substantial performance improvements. These results not only substantiate the effect of the proposed optimization paradigm but also demonstrate its portability and general applicability across KAN variants.

5.7 Discussion

To demonstrate portability across heterogeneous hardware platforms, we evaluate *ChebyKAN* on a consumer-grade RTX 4060 GPU. The results mirror the trend observed on A100, with our optimized kernel reducing latencies by 1.7–2.3× across all configurations.

6 Conclusion

We propose an operator-level optimization design for accelerating polynomial KAN variants on GPUs. Our fused-kernel approach eliminates computational and memory bottlenecks by integrating four techniques: LUT-based basis evaluation, 2D tiling, a two-stage reduction, and coefficient reordering. Compared to the Python-based implementation and the vendor-optimized baseline version, our method significantly improves speed and throughput across three heterogeneous benchmarks. The design generalizes broadly to architectures like ChebyKAN and other polynomial architectures, serving as a reusable component for basis function layers.

References

- [1] Hans M Aus and Granino A Korn. 2006. Table-lookup/interpolation function generation for fixed-point digital computations. *IEEE Trans. Comput.* 100, 8 (2006), 745–749.
- [2] Subhransu S. Bhattacharjee. 2024. TorchKAN: Simplified KAN Model with Variations. GitHub repository. <https://github.com/1ssb/torchkan>
- [3] Alexander Dylan Bodner, Antonio Santiago Tepsich, Jack Natan Spolski, and Santiago Pourteau. 2024. Convolutional kolmogorov-arnold networks. *arXiv preprint arXiv:2406.13155* (2024).
- [4] Sharan Chetlur, Cliff Woolley, Philippe Vandermersch, Jonathan Cohen, John Tran, Bryan Catanzaro, and Evan Shelhamer. 2014. cudnn: Efficient primitives for deep learning. *arXiv preprint arXiv:1410.0759* (2014).
- [5] George Cybenko. 1989. Approximation by superpositions of a sigmoidal function. *Mathematics of control, signals and systems* 2, 4 (1989), 303–314. doi:10.1007/BF02551274
- [6] Lawrence C. Evans. 2010. *Partial Differential Equations* (2nd ed.). Graduate Studies in Mathematics, Vol. 19. American Mathematical Society. doi:10.1090/gsm/019
- [7] Aditya Nalgunda Ganesh. 2024. KAN-GPT: The PyTorch implementation of Generative Pre-trained Transformers (GPTs) using Kolmogorov-Arnold Networks (KANs) for language modeling. GitHub repository. <https://github.com/AdityaNG/kan-gpt> version 1.0.0 (released 2024-05-09).
- [8] GistNoesis. 2024. FusedFourierKAN: C++ & CUDA ops for fused Fourier Kolmogorov-Arnold Networks. GitHub repository. <https://github.com/GistNoesis/FusedFourierKAN>
- [9] Xavier Glorot and Yoshua Bengio. 2010. Understanding the difficulty of training deep feedforward neural networks. In *Proceedings of the thirteenth international conference on artificial intelligence and statistics*. JMLR Workshop and Conference Proceedings, 249–256.
- [10] Bruce Greer, John Harrison, Greg Henry, Wei Li, and Peter Tang. 2001. Scientific computing on the Itanium™ processor. In *Proceedings of the 2001 ACM/IEEE conference on Supercomputing*. 41–41.
- [11] Chunyu Guo, Lucheng Sun, Shilong Li, Zelong Yuan, and Chao Wang. 2024. Physics-informed kolmogorov-arnold network with chebyshev polynomials for fluid mechanics. *arXiv preprint arXiv:2411.04516* (2024).
- [12] Kaggle. 2016. House Prices: Advanced Regression Techniques. Kaggle competition page. <https://www.kaggle.com/competitions/house-prices-advanced-regression-techniques>
- [13] A. N. Kolmogorov. 1963. On the representation of continuous functions of many variables by superposition of continuous functions of one variable and addition. 55–59 pages. doi:10.1090/trans2/028/04
- [14] Yann LeCun, Yoshua Bengio, and Geoffrey Hinton. 2015. Deep learning. *nature* 521, 7553 (2015), 436–444.

- [15] Ziming Liu, Yixuan Wang, Sachin Vaidya, Fabian Ruehle, James Halverson, Marin Soljačić, Thomas Y Hou, and Max Tegmark. 2024. Kan: Kolmogorov-arnold networks. *arXiv preprint arXiv:2404.19756* (2024).
- [16] Vinod Nair and Geoffrey E Hinton. 2010. Rectified linear units improve restricted boltzmann machines. In *Proceedings of the 27th international conference on machine learning (ICML-10)*. 807–814.
- [17] NVIDIA Corporation 2025. *cuBLAS Library User Guide*. NVIDIA Corporation, Santa Clara, CA. https://docs.nvidia.com/cuda/pdf/CUBLAS_Library.pdf
- [18] NVIDIA Corporation 2025. *CUDA Math API Reference Manual* (release 12.9 ed.). NVIDIA Corporation, Santa Clara, CA. https://docs.nvidia.com/cuda/pdf/CUDA_Math_API.pdf Online documentation.
- [19] Cynthia Rudin. 2019. Stop explaining black box machine learning models for high stakes decisions and use interpretable models instead. *Nature machine intelligence* 1, 5 (2019), 206–215.
- [20] David E. Rumelhart, Geoffrey E. Hinton, and Ronald J. Williams. 1986. Learning representations by back-propagating errors. *Nature* (Oct 1986), 533–536. doi:10.1038/323533a0
- [21] Sidharth SS, Keerthana AR, and Anas KP. 2024. Chebyshev polynomial-based kolmogorov-arnold networks: An efficient architecture for non-linear function approximation. *arXiv preprint arXiv:2405.07200* (2024).
- [22] SynodicMonth. 2024. ChebyKAN: Kolmogorov-Arnold Networks using Chebyshev polynomials. GitHub repository. Retrieved 2025-08-13 from <https://github.com/SynodicMonth/ChebyKAN> commit 5f7efdd18e749bcc99481bd87dc90bdeafb920d8.
- [23] Philippe Tillet, Hsiang-Tsung Kung, and David Cox. 2019. Triton: an intermediate language and compiler for tiled neural network computations. In *Proceedings of the 3rd ACM SIGPLAN International Workshop on Machine Learning and Programming Languages*. 10–19.
- [24] Cassia Valentini-Botinhao. 2017. Noisy reverberant speech database for training speech enhancement algorithms and TTS models. Dataset. (2017). <https://datashare.ed.ac.uk/handle/10283/2826> Online dataset.
- [25] Y Wang, J Sun, J Bai, C Anitescu, MS Eshaghi, X Zhuang, T Rabczuk, and Y Liu. 2025. A physics-informed deep learning framework for solving forward and inverse problems based on Kolmogorov–Arnold Networks. *Computer Methods in Applied Mechanics and Engineering* 433 (2025), 117518.
- [26] Pete Warden. 2018. Speech commands: A dataset for limited-vocabulary speech recognition. *arXiv preprint arXiv:1804.03209* (2018).
- [27] Samuel Williams, Andrew Waterman, and David Patterson. 2009. Roofline: an insightful visual performance model for multicore architectures. *Commun. ACM* 52, 4 (2009), 65–76.
- [28] Jinfeng Xu, Zheyu Chen, Jinze Li, Shuo Yang, Wei Wang, Xiping Hu, and Edith C-H Ngai. 2024. FourierKAN-GCF: Fourier Kolmogorov-Arnold Network–An Effective and Efficient Feature Transformation for Graph Collaborative Filtering. *arXiv preprint arXiv:2406.01034* (2024).
- [29] Xingyi Yang and Xinchao Wang. 2024. Kolmogorov-arnold transformer. *arXiv preprint arXiv:2409.10594* (2024).
- [30] Yu-Sen Yang, Ling Guo, and Xiaodan Ren. 2025. Multi-Resolution Training-Enhanced Kolmogorov-Arnold Networks for Multi-Scale PDE Problems. *arXiv preprint arXiv:2507.19888* (2025).
- [31] Runpeng Yu, Weihao Yu, and Xinchao Wang. 2024. Kan or mlp: A fairer comparison. *arXiv preprint arXiv:2407.16674* (2024).
- [32] Fan Zhang and Xin Zhang. 2024. Graphkan: Enhancing feature extraction with graph kolmogorov arnold networks. *arXiv preprint arXiv:2406.13597* (2024).